Magnetic Separation News, 1984, Vol. 1, pp. 67–99
0731-3632/84/0102-0067 $25.00/0
© Gordon and Breach Science Publishers, Inc., 1984
Printed in the United Kingdom

HIGH GRADIENT MAGNETIC GAS FILTRATION

AIK CHONG LUA AND ROBERT F. BOUCHER
Department of Mechanical Engineering, University of Sheffield, Sheffield, S1 3JD, England.

Abstract Highly successful tests have shown that high gradient magnetic filtration can provide a viable alternative to conventional filtration to curb the amount of stack gas particulate emissions from iron-based industries, especially steelmaking processes. Using basic oxygen furnace dust in our work at Sheffield University, filtration efficiencies of 99% and greater were obtained for submicron particles down to an optically measurable 0.24 μm diameter; for particles of 1 μm and above, 100% filtration efficiency was achieved. High gas throughput, together with low pressure losses, low applied magnetic fields and good filter matrix loadability all further indicate the potential commercial practicality of HGMF in the steelmaking industry.

1. INTRODUCTION

Since the first commercial production of kaolin clays using high gradient magnetic separation (HGMS) in 1969, an increasingly growing number of various separation processes using HGMS are reported in the literature. These applications include as diverse as coal desulphurization, mineral beneficiation and the separation of red blood cells from whole blood. A major potential application of dry high gradient magnetic filtration (HGMF) relates to the removal of all fluid-borne particulate matter from gas streams and, in particular, its use as an air-pollution-abatement device for magnetic particles. The role of gaseous magnetic filtration is to

supplement the existing particulate control devices to curb large-scale emissions of particles from industrial sources, particularly the submicron particle size range. These very fine submicron particles are especially harmful as they constitute the greatest inhalation risk. They are responsible for numerous pulmonary diseases as they can penetrate into the respiratory region of the lungs. Also submicron particles tend to remain airborne in the atmosphere for long periods of time, thus contributing to atmospheric haze or smog. Thus, there is a need to develop more economical and better dust control methods for the fine particle size range.

Stack gases arising from steelmaking processes contain vast quantities of particulate matter which need to be removed before the air is released to the atmosphere. The particulate matter in these stack gases has a high iron content and is thus susceptible to HGMF. The current methods used for stack gas clean-up from steelmaking processes are mainly electrostatic precipitation, wet scrubbing and fabric filtration. There are certain important advantages of HGMF over these methods. In most industrial electrostatic precipitators, the negative corona mode of operation is usually used to obtain a higher corona current. For successful operation, electron-absorbing gases have to be present, of which sulphur dioxide is one of the best. Thus, the increasing drive to eliminate sulphurous gas emissions leads to difficulties in the operation of electrostatic precipitators, and HGMF may offer the alternative solution. In the wet scrubbing process, the problem of atmospheric pollution has been turned into a waste water pollution problem. The venturi scrubber which is chiefly used in this process, is highly energy consumptive and thus its operating costs are high. On the other hand, the loaded matrices of a dry HGMF system can be cleaned using a dry technique, e.g. mechanical rapping, infrasonic cleaning[1]. Lastly, fabric filtration suffers from temperature limitations (the maximum operating temperature for

cotton media is about 80°C) and high maintenance costs as filter media have to be replaced regularly. Gas temperatures close to the Curie temperature of the filter matrix are possible with the HGMF process. For ferritic stainless steel wool (AISI Type 430), the Curie temperature is 610°C[2]. The gas velocity through the fabric filter is generally low; in the range 0.01 to 0.6 m/s whilst gas velocities up to 13.6 m/s were reported by Lua and Boucher[3] for HGMF tests on basic oxygen furnace dust. Hence, a baghouse system is area extensive whilst an HGMF unit is compact for the same quantities of gas to be cleaned.

Dry HGMF has potential applications in other processes where weakly magnetic or paramagnetic particles are to be removed. In the nuclear industry, HGMF can be used to remove radioactive particles, consisting mainly of various oxides of iron, in the primary cooling circuits of gas-cooled reactors. Also in nuclear fuel reprocessing plants, radioactive paramagnetic particles are present as a result of certain shearing and laser cutting processes; these gases or fumes can be cleaned by means of HGMF techniques. HGMF devices are attractive to the nuclear industry because they can withstand high temperatures, pressurization, fires and explosions much better than the high efficiency particulate air filters presently used; further HGMF matrices are cleanable thus reducing active-waste disposal problems. Other possible dry HGMF and HGMS applications are the removal of iron oxide particles in gas-carrying pipelines; the recovery of magnetite from coal fly ash; the recovery of glass from municipal incinerator residues by removing the iron-bearing compounds; the beneficiation of iron ores; and the capture of respirable asbestos fibres in working environments.

2. HGMF OF FINE PARTICLES FROM STEELMAKING STACK GASES

Many of the steelmaking processes produce large emissions of fumes

have to be removed before the stack gases are discharged to the atmosphere. The total iron concentration from several of these processes[4] is as follows: basic oxygen furnace (55 - 70%); open hearth furnace (55 - 70%); scarfing process (50 - 70%); blast furnace (35 -50%); and sintering process (25 - 50%).

In 1975, the Research Triangle Institute (RTI), North Carolina, U.S.A., carried out an investigation for the U.S. Environmental Protection Agency to determine if HGMF technology could be applied to control fine particle emissions from steelmaking processes[5]. A laboratory pilot plant was constructed and tests were carried out for two types of dust viz. basic oxygen furnace (BOF) dust and electric arc furnace (EAF) dust. The schematic diagram of the laboratory pilot plant is shown in Fig.1. The dust is dispersed into the air stream of the 61-cm diameter wind tunnel using a fluidized-bed dust generator. A slipstream of the dust-laden air is drawn off the wind tunnel into the HGMS device. Before the HGMF filter, the stream passes through a

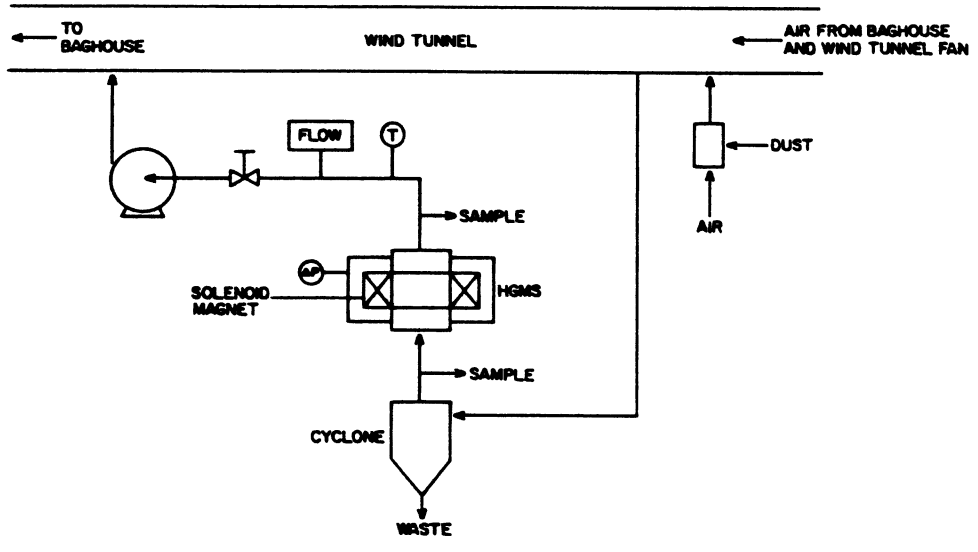

FIGURE 1 Schematic diagram of the RTI HGMF laboratory pilot plant (after Gooding et al, ref. 5)

cyclone (a 50-percent cut point of about 5 μm) to remove large particles. As the air stream flows upwards through the cyclone, a baffle is installed to break up the vortex. Upstream and downstream of the filter, dust samples are extracted to determine particle sizes and concentrations. After the downstream sample ports, the clean air stream passes through a blast gate which is used for flow control, through a booster fan and back into the wind tunnel loop. A pitot tube is located between the downstream sample ports and the blast gate to determine the average downstream flow velocity. All particle sizes and concentrations were determined using MRI Model 1502 inertial cascade impactors (manufactured by Meteorology Research, Inc., California, U.S.A.) except for the two long term matrix loadability tests. In these two tests, an optical particle counter, Climet Model 208A (Climet Instruments Co., California, U.S.A) was used, together with a dilution system to avoid particle coincidence losses in the counter. AISI 430 ribbon-shaped stainless steel wires were used.

The magnetization curves for both the BOF and EAF dusts are shown in Fig. 2. Filter penetration values were computed from particle sizes and concentrations at filter inlet and outlet. Figures 3 and 4 show the matrix loadabilities for the BOF and EAF dusts respectively, starting from clean matrices in both tests. The BOF data shows no deterioration in efficiency during the test period even though the matrix has collected about twice its own mass of dust. On the other hand, the EAF dust which has a lower specific magnetization than the BOF dust, shows gradual deterioration in collection efficiency with loading from the start. At the end of the EAF test, the matrix had collected about three times its own mass of dust. However, extreme deviations from isokinetic sampling are apparent in the way Gooding et al[5] carried out the two loading tests for Figs. 3 and4. The air velocity just ahead of the sampling nozzle was not determined. Instead a constant sampling velocity of approximately 5.0 m/s was assumed and

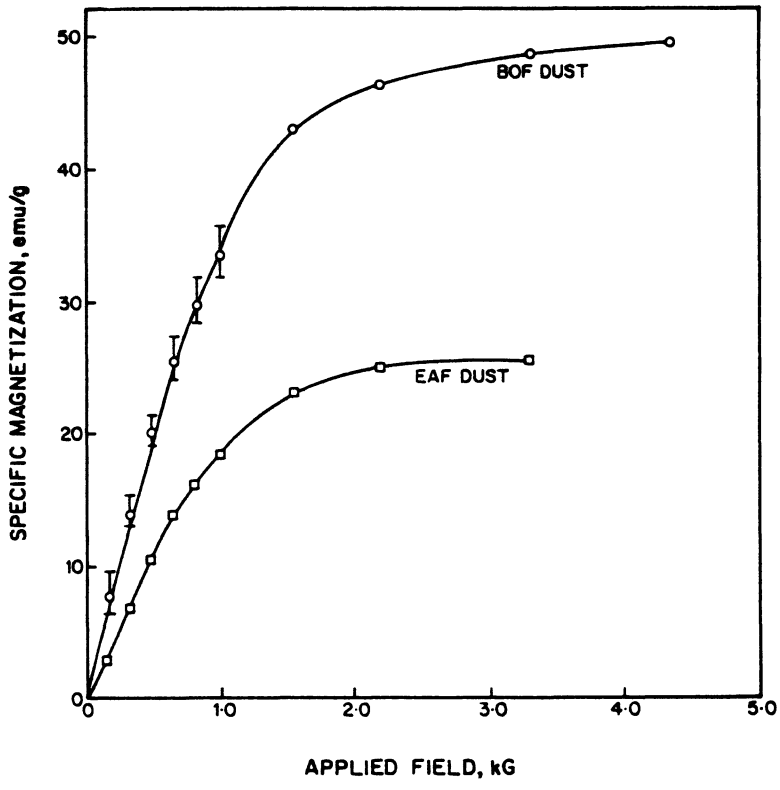

FIGURE 2 Magnetization curves of BOF and EAF dusts (after Gooding et al, ref. 5)

used throughout in both tests even though these tests were conducted at a constant superficial air velocity of 8.2 m/s. Also, the sampled dust aerosols were passed through a small cyclone (with a 50-percent cut point of about 1 μm) and then into a dilution system before any particle measurements were carried out using the optical particle counter. Such measurements of particle sizes and concentrations would surely be vastly different from those actually entering and leaving the HGMF filter, even for small particle sizes.

Gooding et al[5] also investigated the effects of various parameters viz. matrix packing density, magnetic field and gas velocity on filter performance. Increasing the matrix length shows

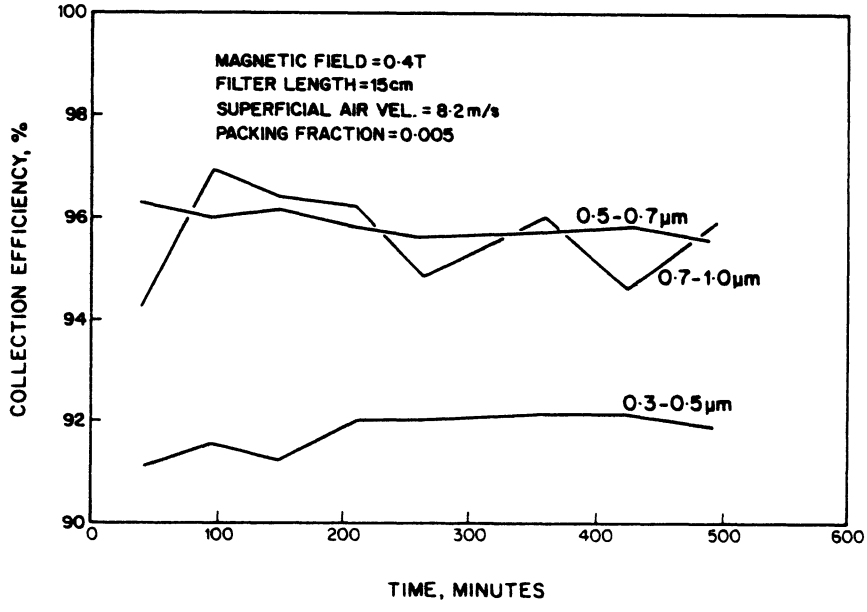

FIGURE 3 Matrix loadability for BOF dust (after Gooding et al, ref. 5)

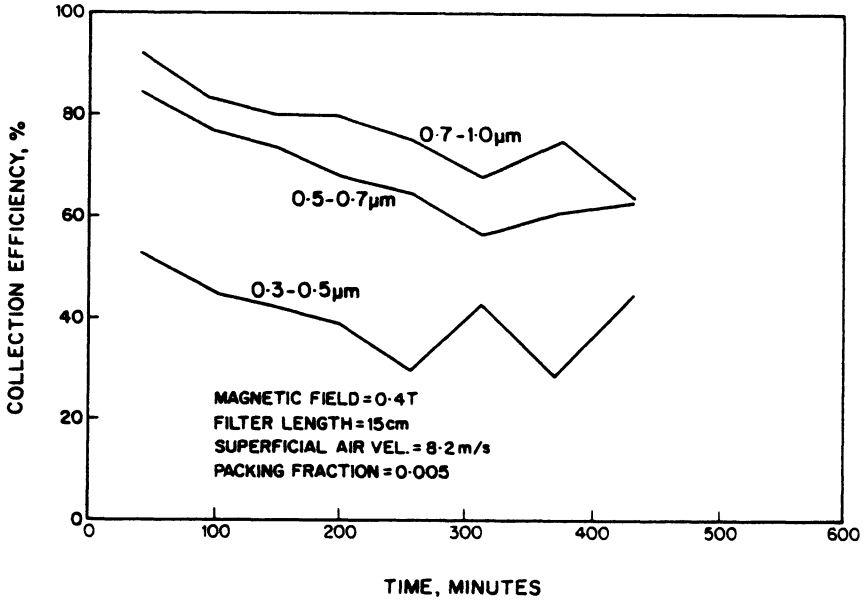

FIGURE 4 Matrix loadability for EAF dust (after Gooding et al, ref. 5)

a general trend of decreasing filter penetration (Fig. 5). Penetration is defined as the ratio of particle concentration at filter outlet to that at inlet. Theoretical consideration of the filter penetration equation (i.e. $P = \exp. \{-\frac{4FLR_c}{\pi^2 a(1-F)}\}$ where P = filter penetration, F = volume packing fraction of matrix, L = filter length, R_c = dimensionless capture radius of single wire, a = wire radius) suggests that doubling the matrix length should result in squaring the penetration. The improvement with the longer matrix in Fig. 5 is not as significant as should have been predicted by the penetration equation. The effect of matrix packing density is shown in Fig. 6. Increasing the packing density reduces the penetration. The improvement in efficiency achieved by doubling the packing density is greater than predicted by the filter penetration equation. The effects of applied magnetic

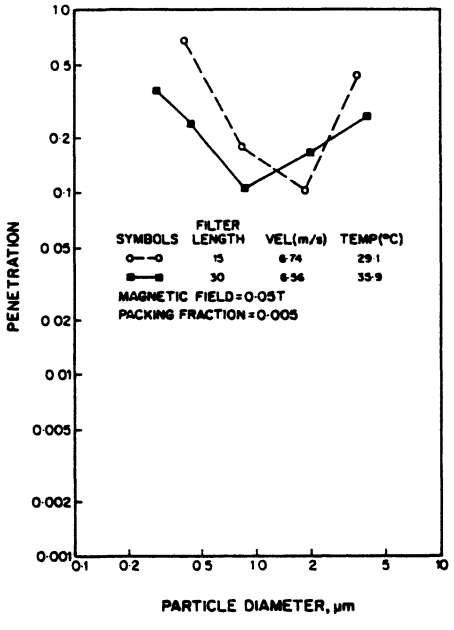

FIGURE 5 Effect of matrix length on filter penetration for BOF dust (after Gooding et al, ref. 5)

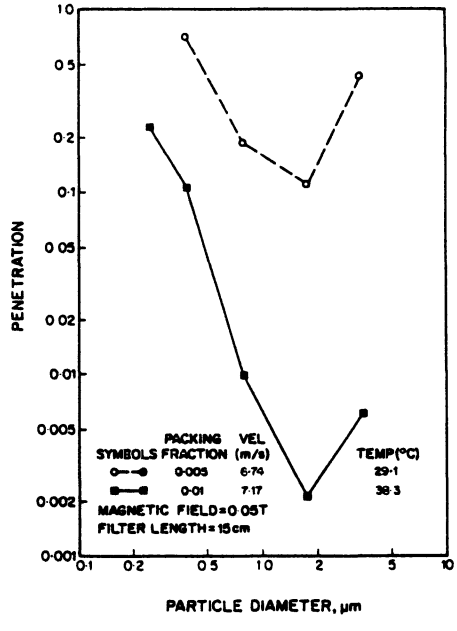

FIGURE 6 Effect of matrix packing density on filter penetration for BOF dust (after Gooding et al, ref. 5)

fields on filter penetration for the BOF and EAF dusts are shown in Figs. 7 and 8 respectively. The random scatters in the experimental results for both dusts do not show any definite trend. Theoretically, increasing the magnetic field (before both the wire and particle saturate) increases the wire and particle magnetizations which enhance particle capture, if the other parameters remain unchanged. Figure 9 shows the effect of superficial air velocity. Increasing velocity does not seem to have a strong effect on the smaller particles but detrimental to larger particles.

The generally wide scatters in the experimental results of Gooding et al[5] viz. Figs.5 - 9, could be attributed partly to the choice of the particle measurement method - the inertial cascade impactor. Its use is associated with many sources of error[6]. The

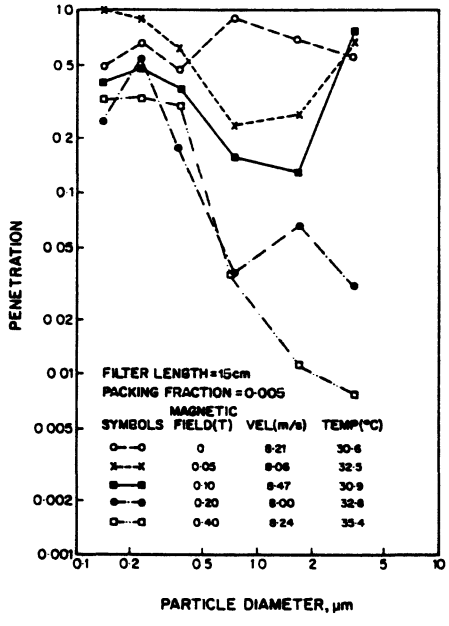

FIGURE 7 Effect of applied magnetic field on filter penetration for BOF dust (after Gooding et al, ref. 5)

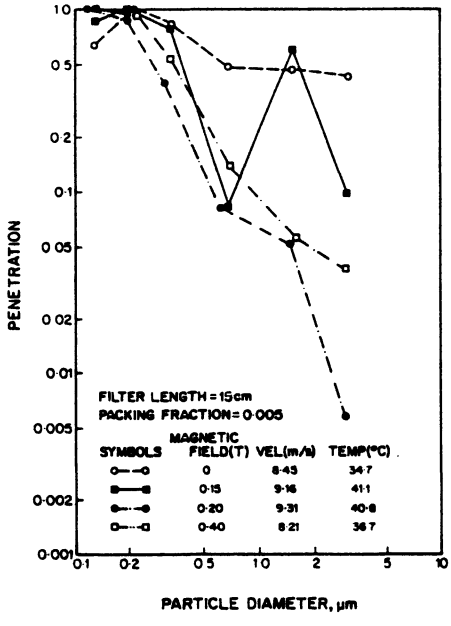

FIGURE 8 Effect of applied magnetic field on filter penetration for EAF dust (after Gooding et al, ref. 5)

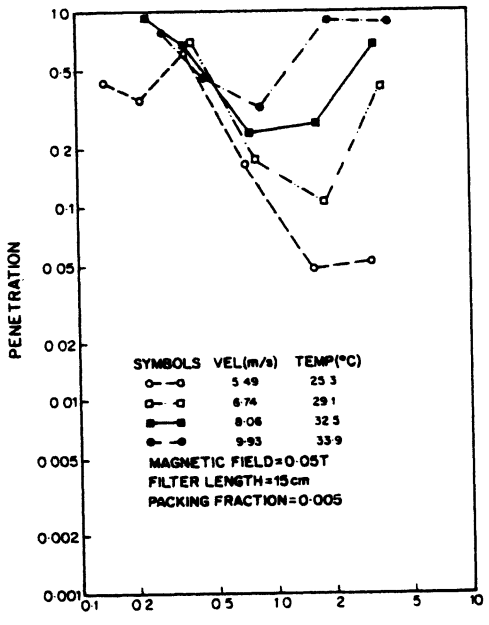

FIGURE 9 Effect of superficial air velocity on filter penetration for BOF dust (after Gooding et al, ref. 5)

main sources of errors in cascade impactors are particle depositions on the walls between the stages, on the walls of nozzles and on perforated plates in multi-jet cascade impactors particularly the deposition of large particles on the first perforated plate in which the inlet pipe acts as a nozzle and the first perforated plate as an impaction plate. As particles are collected in localized deposits on the impaction plate and as these deposits become overloaded, incoming particles will bounce off the previously deposited particles. Also, when the dust deposit reaches a sufficient thickness, it can be blown off and be re-entrained in the air stream and thereafter deposits on the lower impactor stages causing spurious results, e.g. a 3 μm particle will appear by gravimetric analysis to represent 1000 particles of 0.3 μm diameter. A number concentration analysis rather than a gravimetric analysis will be more ideal for small particles for avoiding long sampling period in order to obtain weighable quantity

of dust, especially submicron particle analysis downstream of a highly efficient filter.

Another possible reason for such spread of experimental results in Figs. 5 - 9 could be due to the experimental techniques employed by Gooding et al[5]. Likewise for these efficiency tests as in the loadability tests (Figs.3 and 4), the velocity profiles upstream and downstream of the HGMF filter were not determined prior to sampling into the cascade impactor. A sampling velocity based on the filter downstream average velocity was used throughout for all the sampling positions. But, it must be highly likely that the velocity profile at the filter upstream sampling position would be greatly distorted and irregular after the flow had passed through the cyclone. Also the characteristic swirling flow of the cyclone might not be cured completely by means of a baffle as used by Gooding et al[5]. Thus, the velocity at any sampling position could be vastly different from the downstream average velocity value. Similarly for the downstream side, the velocity profile would also be highly non-uniform after passing through the random matrix configuration as was observed in similar HGMF work at Sheffield University[7]. Hence, anisokinetic sampling might have also contributed to such scatters in Figs. 5 - 9.

Gooding[4] conducted an impressive on-site testing of a pilot HGMF plant on a sinter plant in Pennsylvania, U.S.A. In the production of iron, the sintering process is used to combine iron ore fines with flux in the form of limestone or dolomite and with other iron-bearing materials such as flue dust, mill scale, turnings and borings to form a blast furnace feed material of appropriate composition and size. In the pilot plant, a slipstream from the windbox exhaust of the sinter plant was drawn into and through the HGMF filter. However, the pilot plant did not achieve a satisfactory level of filtration efficiency because of the extremely low magetization value of the sinter dust that actually reached the HGMF filter. Samples obtained at the filter inlet

showed a saturation magnetization of 2.4 emu/g at 0.3 Tesla compared to 9 emu/g for samples obtained from the plant precipitator hoppers. Moreover, the saturation magnetization of this sinter dust at the HGMF filter inlet was only 1/20 that of the BOF dust reported earlier[5]. The larger sinter dust particles were believed to be higher in iron content but substantial quantities of these particles did not reach the HGMF filter due to gravitational settling in the slipstream upstream of the HGMF filter and also possibly less large particles were drawn from the windbox exhaust. Size measurements and subsequent chemical analyses revealed the outlet dust after the HGMF filter contained a high percentage of very fine particles of alkali chlorides which would not be captured by a magnetic filter. Thus, for future on-site evaluation of a pilot HGMF plant, suitable industrial emissions have to be identified, dust characterization and laboratory HGMF tests have to be carried out on the actual source prior to setting up the pilot plant.

Drawing on the set-backs by Gooding et al[5], a thorough and careful HGMF investigation on BOF dust was carried out by Lua[7] for his Ph.D dissertation. The individual effects of a wide range of operating parameters - matrix volume packing fraction, filter length, magnetic field, gas velocity, wire size and wire aspect ratio (for rectangular wires) on the filtration efficiency of the HGMF filter were investigated. It was also desirable to determine the matrix dust load capacity or loadability for the BOF dust under different combinations of these parameters

The schematic set-up of the HGMF test rig is shown in Fig. 10. Room air is drawn into the 98.4 mm diameter copper duct by a main centrifugal fan and a smaller fan within the fabric bag unit. Air flow in the duct is adjusted by 2 flow dampers. The pre-filter and absolute filter at the duct entrance clean the incoming air. Slightly downstream of the absolute filter, BOF dust particles are injected into the main airstream. The particles are generated by

an aerosol generator which uses the fluidized bed technique to thoroughly deagglomerate the dust particles before elutriation. The aerosol generator has been tested and found to be capable of fully dispersing the particles as single particles at steady output for long periods of time, the details and performance of which are reported elsewhere[8]. Located above the fluidized bed, an aerosol neutralizer (Model 3054, Thermo-Systems Inc., Minnesota, U.S.A.) neutralizes any static charges acquired by the aerosolized particles during the fluidization process. It contains a sealed source of 10 millicuries of krypton - 85 gas.

The filter matrix consisting of random stainless steel wires (AISI 430) of rectangular cross-sections, is located at approximately 6.5 m downstream of the duct entrance, in the 113 mm bore of a water-cooled compensated solenoid magnet. This self-built 31.7 cm long solenoid magnet, with an inside notched compensated coil, has a very homogeneous field distribution; a variation of only 1.6% along a 15 cm length central region of the bore. Wall static tappings across the matrix are used to determine the filter

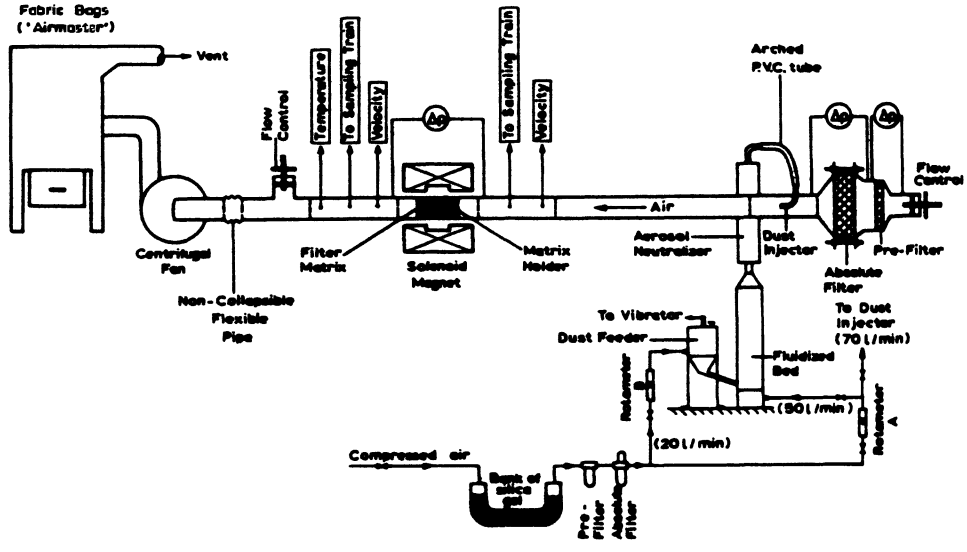

FIGURE 10 Schematic set-up of HGMF test rig

resistance. Upstream and downstream of the matrix, velocity profiles were determined with a pitot tube and wall static tappings (in accordance with BS1042: Part 2A: Aug. 1973) to obtain isokinetic sampling rates as well as the average air velocity in the duct. Sampling ports are located upstream and downstream of the matrix. Also in the downstream section of the duct, a thermometer is inserted for reading the air temperature. After the main centrifugal fan, a filter unit consisting of fabric bags cleans the air, if necessary, before discharging to atmosphere.

Particle sizes and concentrations upstream and downstream of the matrix were determined by an optical particle spectrometer, CSASP-100-HC (Particle Measuring Systems, Inc., Colorado, U.S.A.). The spectrometer employs a multi-mode laser light source for particle illumination. It eliminates errors associated with diluting the sample or passing it through a micro-jet before optical analysis. The 10 mm diameter flow in the inlet tube is retained throughout, and particles are analysed in a small optically determined area at the centre of this stream. The instrument was calibrated by the manufacturers and checked during the present investigation using Dow latex particles, and found to be accurate. It covers the size range 0.24-7.0 μm in 3 overlapping sub-ranges with 15 sizes in each sub-range. A gravimetric particle size analysis, such as the use of an inertial cascade impactor, was avoided in anticipation of substantial errors, especially with sub-micron particle sizes, as discussed earlier in relation to the work by Gooding et al[5]. The schematic arrangement of the sampling train for the optical particle spectrometer analysis is shown in Fig.11. For scanning electron microscope examination of particle characteristics, samples were collected on a 47 mm diameter Nuclepore polycarbonate membrane filter, pore size 0.8 μm, using the filter sampling train shown in Fig. 12.

The BOF test dust used was collected dry at the stack of a steelmaking plant. The dust was milled, dried completely and

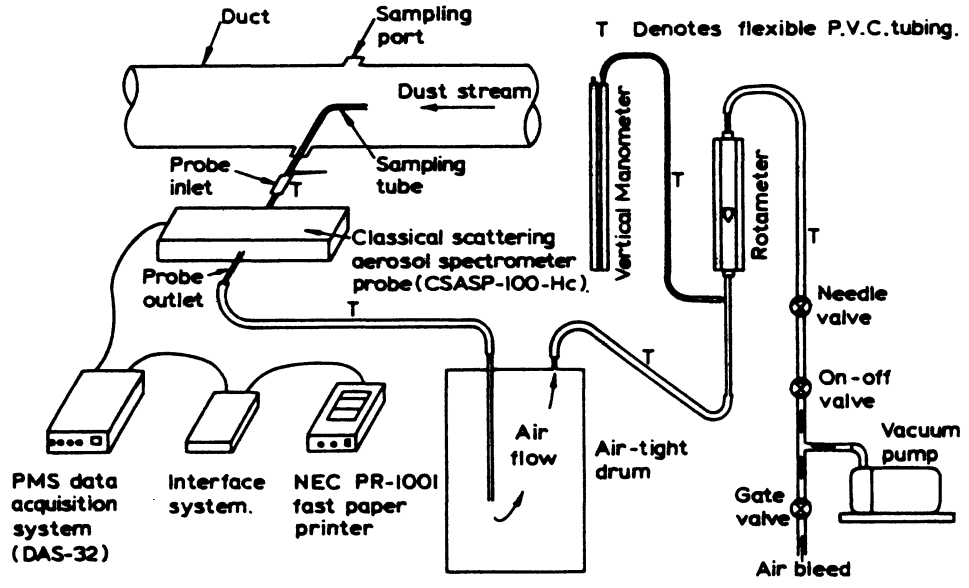

FIGURE 11 Schematic arrangement of the sampling train for optical particle spectrometer analysis

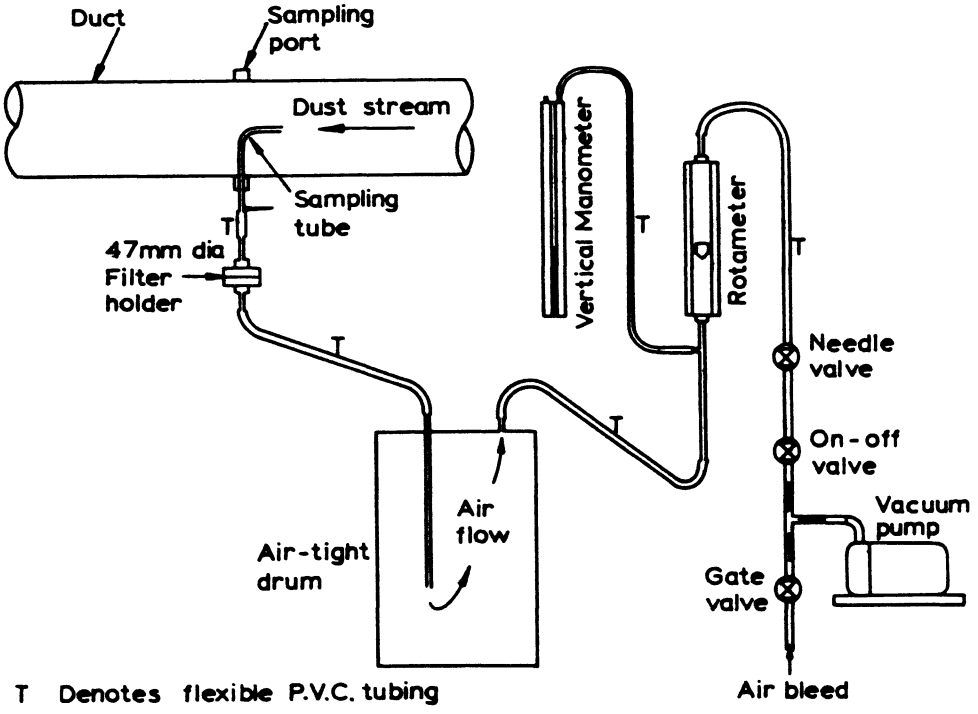

FIGURE 12 Schematic arrangement of the filter sampling train

sieved to size range below 300 μm before it was dispersed into the test duct by the aerosol generator. Scanning electron micrographs of dust particles (Fig. 13) show that the particles are fully dispersed as single particles. The particle size distribution of the BOF dust is shown in Fig. 14. It shows the particle sizes are below 2 μm diameter, mainly in the submicron range. Figure 15 shows the relationship between the particle magnetization and the magnetic field for the BOF dust. The particle magnetization tends to a saturation value at an applied field of about 0.3 Tesla. Consequently, the particle magnetic susceptibility tends to an asymptotic value for increasing magnetic fields (Fig. 16). Thus, these data show that BOF dust is ferromagnetic. A spectrographic analysis shows that the iron content of the BOF dust consists of 53% and 5% by weight of Fe_3O_4 and Fe_2O_3 respectively. The other constituents are ZnO, PbO, MnO, SiO_2 and traces of various other chemical compounds.

AISI Type 430 stainless steel wool, consisting of ribbon-shaped rectangular wires, was used for the matrix. Four grades of wires, differing in size and aspect ratio, were tested. The dimensions of these wires are given in Table I. The hydraulic radius is defined as a ratio of twice the cross-sectional area to the wetted perimeter, whilst the aspect ratio is the ratio of width to thickness.

Table I. Dimensions of different grades of wire.

Grade	Width (μm)	Thickness (μm)	Hydraulic radius (μm)	Aspect ratio
00	112	48	33.5	2.33
0	135	38	29.5	3.55
2	165	69	48.5	2.39
4	198	97	65.0	2.04

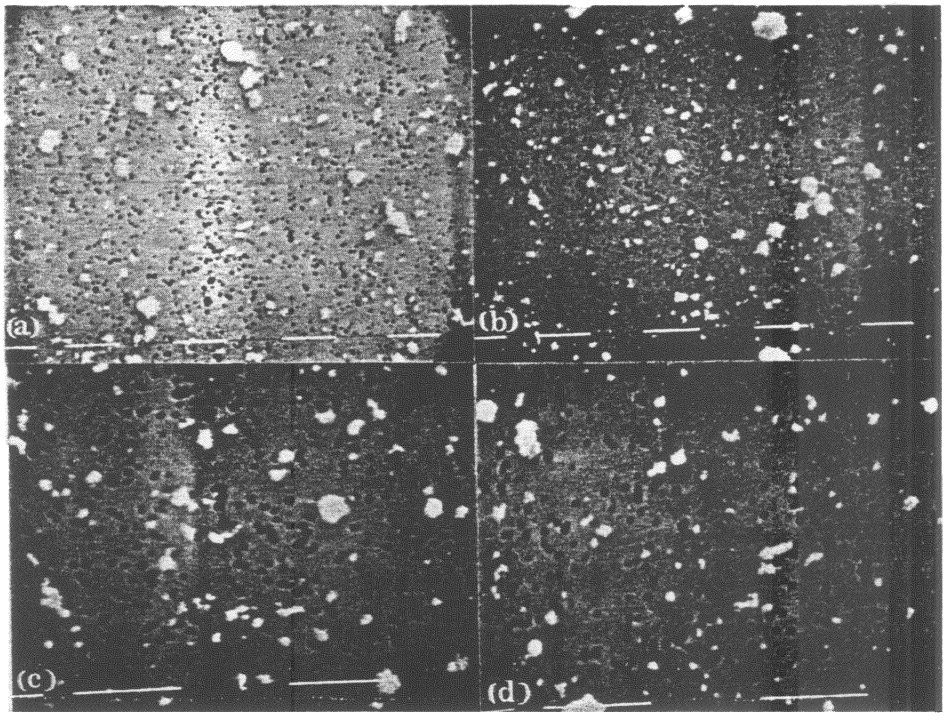

FIGURE 13 Scanning electron micrographs of BOF dust particles: (a) and (b) 1250X, white bar spacing = 10 μm; (c) and (d) 2500X, white bar spacing = 10 μm

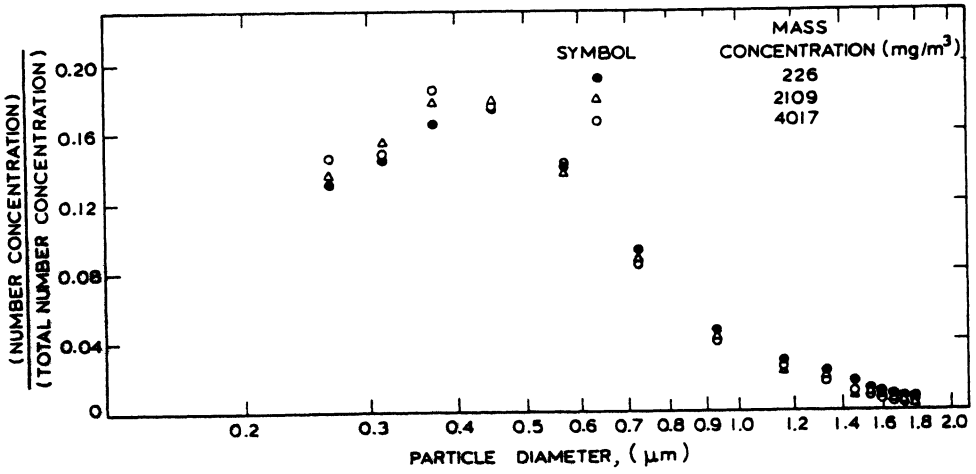

FIGURE 14 Normalized BOF particle size distribution

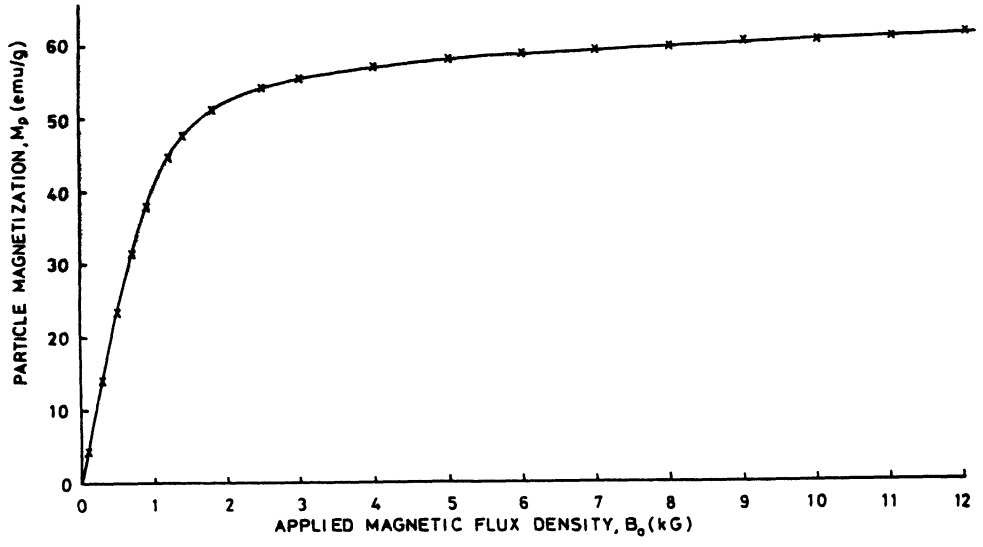

FIGURE 15 Magnetization curve for BOF dust

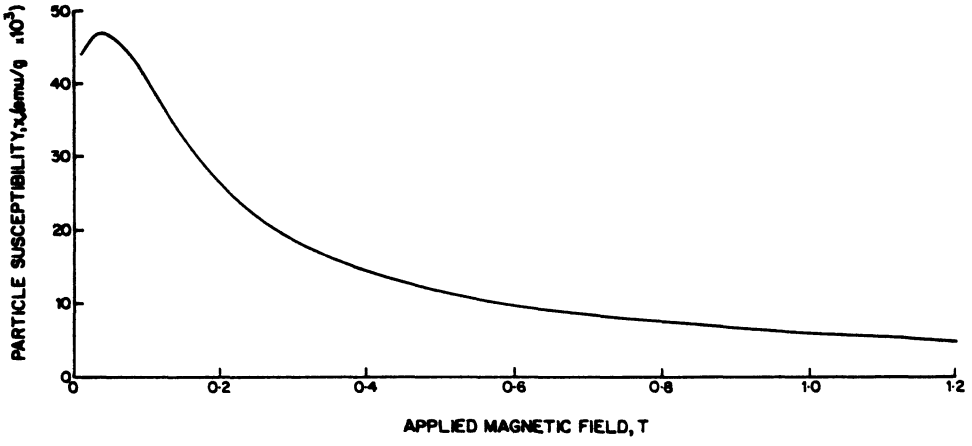

FIGURE 16 Magnetic susceptibility of BOF dust

To study the performance of the HGMF filter with dust loading, long-term tests were carried out. Dust particles were sampled isokinetically and continuously from the centre of the duct into the optical particle spectrometer, downstream of the matrix. Pressure drop across the matrix was recorded at regular intervals. Sampling was stopped when the penetration of the smaller particles was becoming excessive. The matrix was removed for gravimetric analysis. Upstream sampling, without the matrix, was carried out both before and after downstream sampling to obtain an average upstream particle concentration for computing filtration efficiencies. Figures 17 ,18 and 19 show the matrix loadability for magnetic fields of 0.05, 0.4 and 0.8 Tesla respectively, with all the other operating parameters remaining constant. As expected,increasing magnetic field increases the filtration efficiency for all particle sizes shown before loading effects become significant and lead to deterioration of efficiency, especially for the smaller particle sizes.

For a very low field of 0.05 Tesla (Fig.17), the filtration efficiency for all particle sizes shows only modest deterioration up to the stage when the matrix has collected about 2 times its own

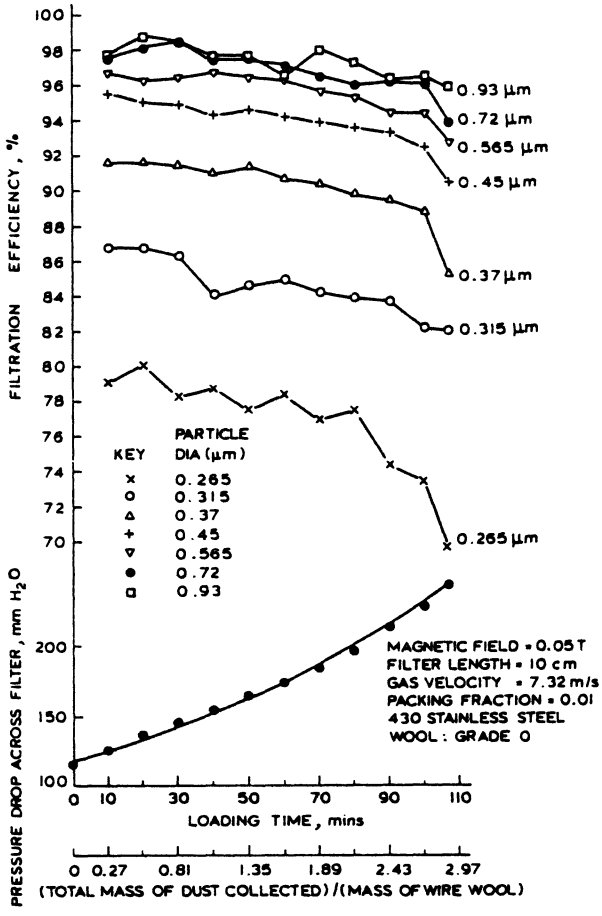

FIGURE 17 Matrix loadability at 0.05 Tesla

mass of dust. Larger captured BOF particles create their own local gradients thus becoming improved sites for further capture, almost maintaining filtration efficiency despite such dust loading. A deterioration in the filtration efficiency is clearly evident for the smallest particles (0.265 μm) thereafter, and for all particles when the matrix has collected about 3 times its own mass of dust. The total amount of dust collected at the end of the test was 162.8 g, a mass ratio of 2.89 (mass of dust collected to mass of wire wool) or a volume ratio 4.72.

At 0.4 Tesla (Fig. 18), the higher filtration efficiency is sustained for all the particle sizes until the matrix holds twice its own mass of dust. Thereafter it suffers significant deterioration only for the smallest two particle sizes up to the maximum loading tested of 216.2 g, a mass ratio of 3.84 and volume ratio of 6.27. The higher applied field thus endows good loadability, providing high efficiency with high dust loading.

At 0.8 Tesla (Fig.19), significant deterioration in filtration efficiency occurs at lower matrix loading (mass ratio 1.5) than at 0.4 Tesla, but from a higher initial level. For loading mass ratios of 2 and greater, the efficiencies for these two fields are almost identical for all but the smallest (0.265 μm) particles, for which it is worse with the higher field. Since the particles approach

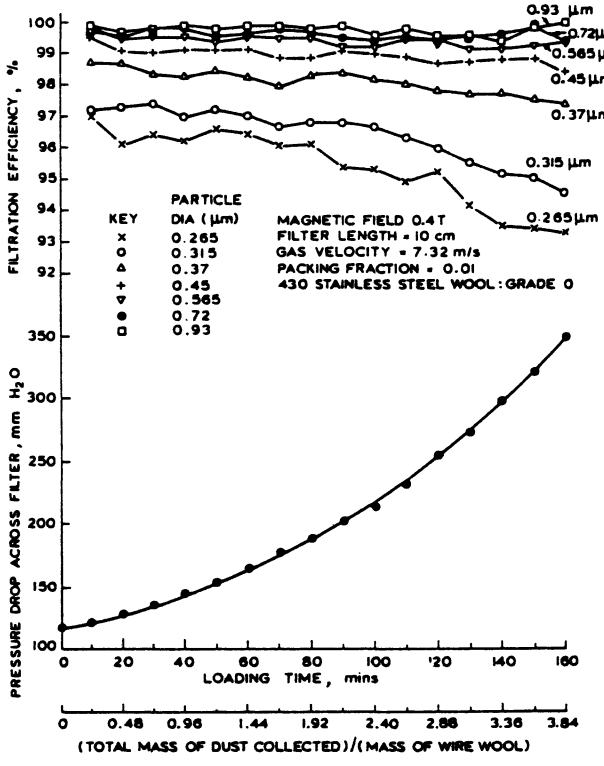

FIGURE 18 Matrix loadability at 0.4 Tesla

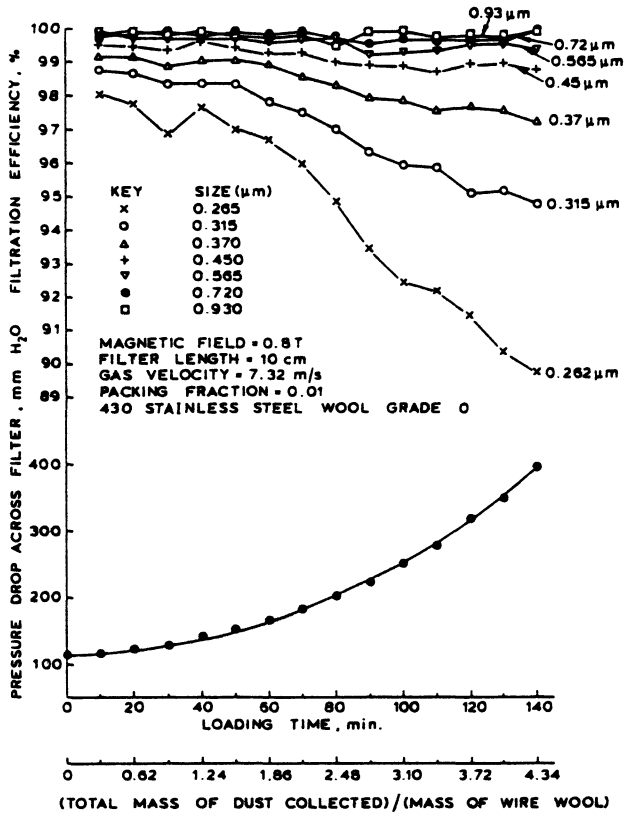

FIGURE 19 Matrix loadability at 0.8 Tesla

saturation at above 0.2 Tesla, the general conclusion is that little or no further improvement in loadability is to be obtained beyond such field levels.

There is good agreement in the pressure drop versus matrix mass load ratio of Figs.17-19. For the heaviest loading of 4.34 mass ratio (7.17 volume ratio) the pressure loss has multiplied 3.5 times. Thus, substantial geometrical distortion which results in reduced magnetic gradients, appears to be the primary factor reducing efficiency. The reduced efficiency is unlikely to arise either from re-entrainment (since no large particle agglomerations were detected by the particle spectrometer) or from particle bounce-off which produces highly erratic results.

Figure 20 shows the matrix loadability without a magnetic field. Although the initial filtration efficiency for all particles is high, rapid fall occurs very soon afterwards with hardly any dust collected in the matrix; the fall is most marked for the smallest size. This very low matrix loadability can also be observed from the flat pressure drop curve. The total amount of dust collected was only 2.3 g (mass ratio 0.041 or volume ratio 0.067) thus demonstrating the importance of an applied magnetic field to both initial and sustained particle capture.

The matrix loadability for a lower packing fraction is shown in Fig. 21. The filtration efficiency is maintained over all particle sizes up to the maximum loading tested (166.6 g)

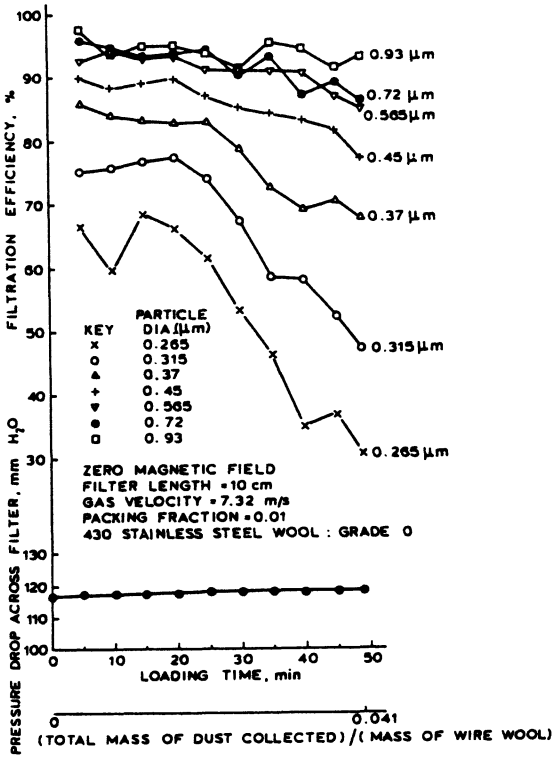

FIGURE 20 Matrix loadability without a field

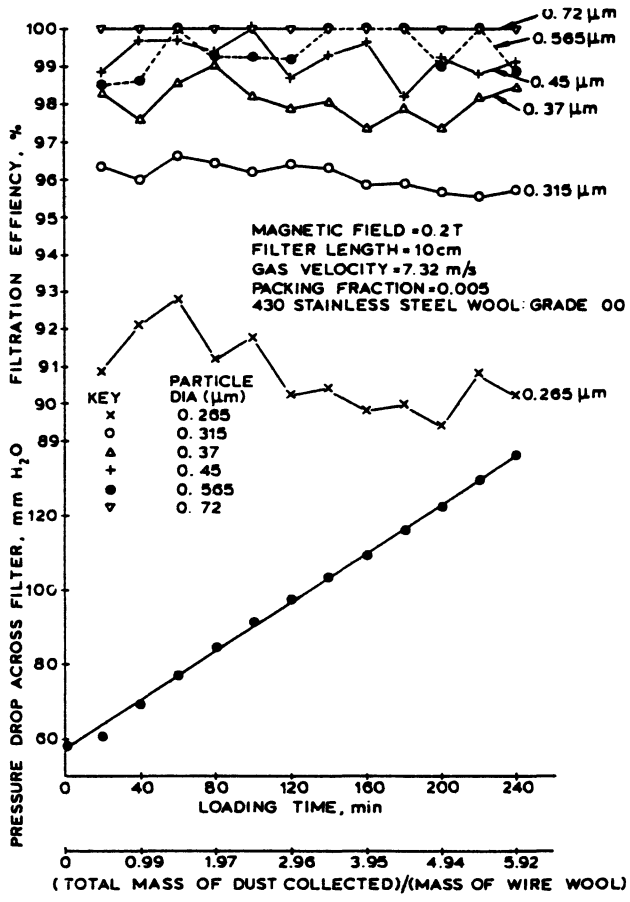

FIGURE 21 Matrix loadability at 7.32 m/s

corresponding to a mass ratio 5.92 or volume ratio 9.66 times that of the wire. This matrix loading (packing fraction 0.005) is higher than those for Figs. 18 and 19 (packing fraction 0.01). The reduced loading for the higher packing fraction is probably due to increased wire-wire interference which is detrimental to particle capture[3]. Furthermore, despite the extremely high loading in Fig. 21, the filter resistance doubles slightly, again benefitting from greater wire separation.

Figure 22 shows loading under the same conditions as Fig. 21 except that the velocity is increased from 7.32 to 11.51 m/s. The

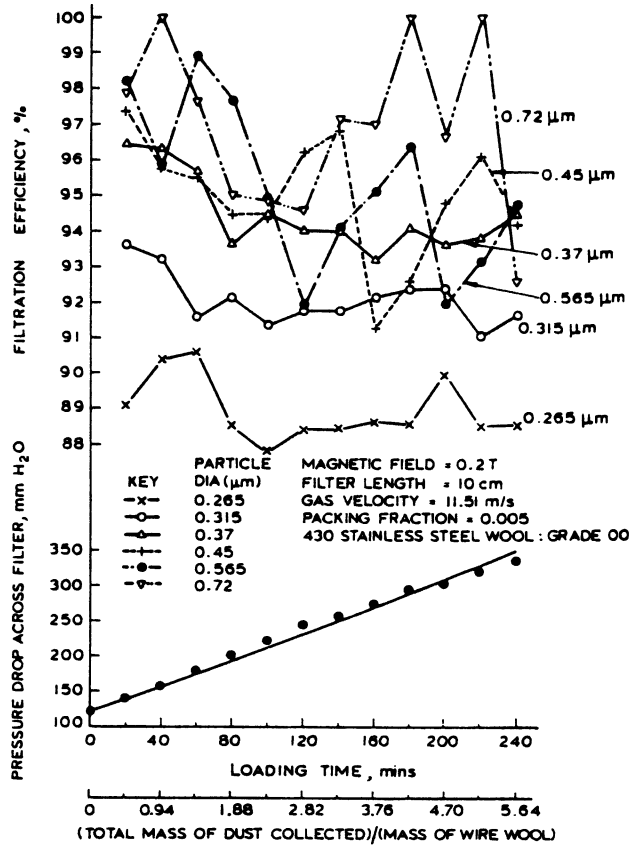

FIGURE 22 Matrix loadability at 11.51 m/s

filtration efficiency, although lower, is again sustained for the smaller particles as the matrix loads up. For the larger particles, however, a secondary effect of particle bounce-off from the collector surface is thought to occur when the ratio of magnetic to inertia forces at impact is less than a critical value. The particle is then carried away if the magnetic forces are too small to overcome the viscous forces in the absence of forward particle inertia. This is quite distinct from re-entrainment where captured particles are later torn off the collector surface, producing agglomerations appearing to be large size particles. In Fig. 22, particle bounce-off occurs at the outset and continues for

all loadings, producing erratic fluctuations, although good average efficiency is still maintained. Despite the excessive velocity, no large particles outside the range dispersed were detected within the 7 μm capacity of the particle spectrometer, suggesting that re-entrainment of particle agglomerations played no part in the fluctuations.

For the HGMF filter efficiency tests, sequential 8-point isokinetic dust samplings were carried out, both upstream and downstream of the matrix, for 30 min at each point. The sample was analysed by the particle spectrometer for particle sizes and number concentrations. The effect of varying one basic parameter at a time on the filter performance was examined with respect to the particle size.

The effect of applied magnetic field on the filtration efficiency is shown in Fig. 23 for grade 00 wire wool. Increasing

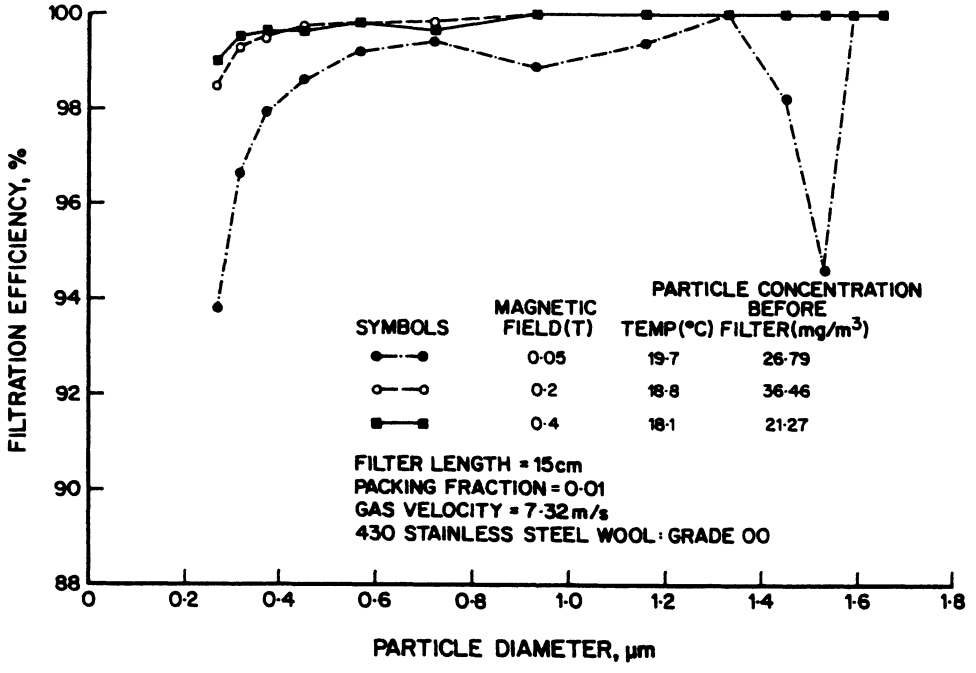

FIGURE 23 Effect of applied magnetic field on filtration efficiency

magnetic field improves the efficiency. The improvement is only marginal for substantial increase above 0.2 Tesla where the particle magnetization approaches its saturation value (Fig. 15). At 0.05 Tesla, it shows a decrease in filtration efficiency for 0.93 μm and larger particles. However, the efficiency should never fall below that of small particles. This phenomenon again suggests particle bounce-off rather than re-entrainment which produces large particle agglomerates. None were detected within the 7 μm capacity of the spectrometer.

The effect of filter length on the filtration efficiency is shown in Fig. 24. Extra length improves efficiency for increasingly smaller particles, above which the length is

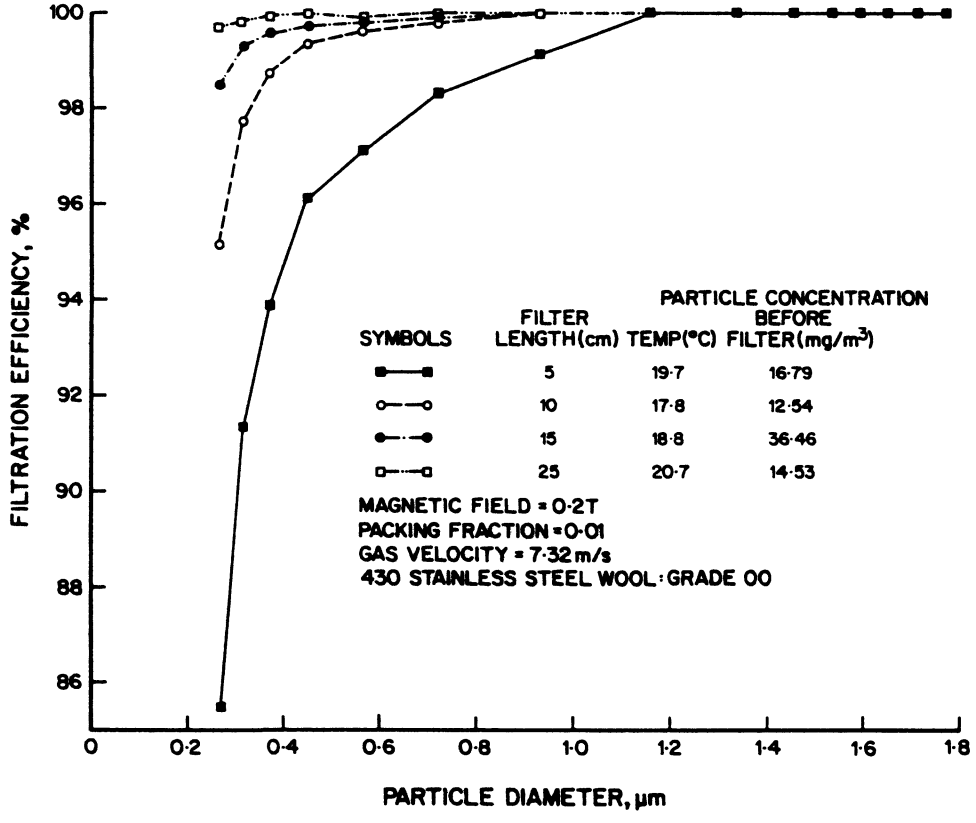

FIGURE 24 Effect of filter length on filtration efficiency

overgenerous. By examining the filter penetration equation i.e. $P = \exp.\{-\frac{4FLR_c}{\pi^2 a(1-F)}\}$, doubling the filter length should result in squaring the penetration. But, from analysing the curves for the 5 cm and 10 cm filter lengths, the reduction in penetration for doubling the length is less dramatic, thus showing the same general trend as observed by Gooding et al (Fig. 5). The effect of volume packing fraction of the matrix on the filtration efficiency is shown in Fig. 25 for wire wool grade 0. Increasing the packing fraction improves the filtration efficiency throughout. But, the decrease in penetration for increasing packing fraction is generally less than that predicted by the filter penetration equation. Thus, increasing packing fraction very often lowers the effectiveness of individual wires in a filter, due primarily to increased wire shadowing and magnetic interference effects[3].

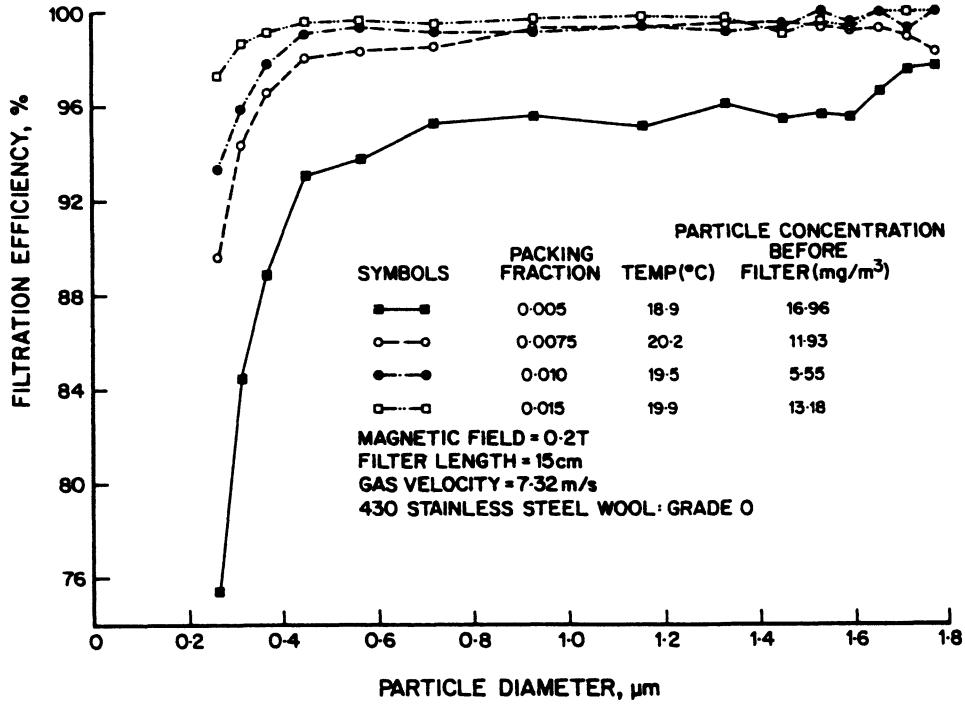

FIGURE 25 Effect of matrix packing fraction on filtration efficiency

The effect of increased gas velocity on the filtration efficiency is shown in Fig. 26. (In the inertial regime, if the capture radius is less than the wire radius, particles should have an increased likelihood of capture at higher velocities due to their higher inertia.) In Fig. 26, increased velocity generally produces improved capture efficiency, thus demonstrating the significance of particle inertia. At 13.62 m/s between 0.565-1.155 μm, the deterioration in efficiency is another manifestation of particle bounce-off in which at these higher velocities, the ratio of magnetic to inertial forces is reduced. Above 1.33μm, either adequate matrix length or the highly favourable filter front face (which is discussed later) ensures particle capture.

The effects of wire size and aspect ratio on the filtration efficiency are shown in Fig. 27 for a given packing fraction of 0.01. Decreasing wire size with approximately the same aspect ratio

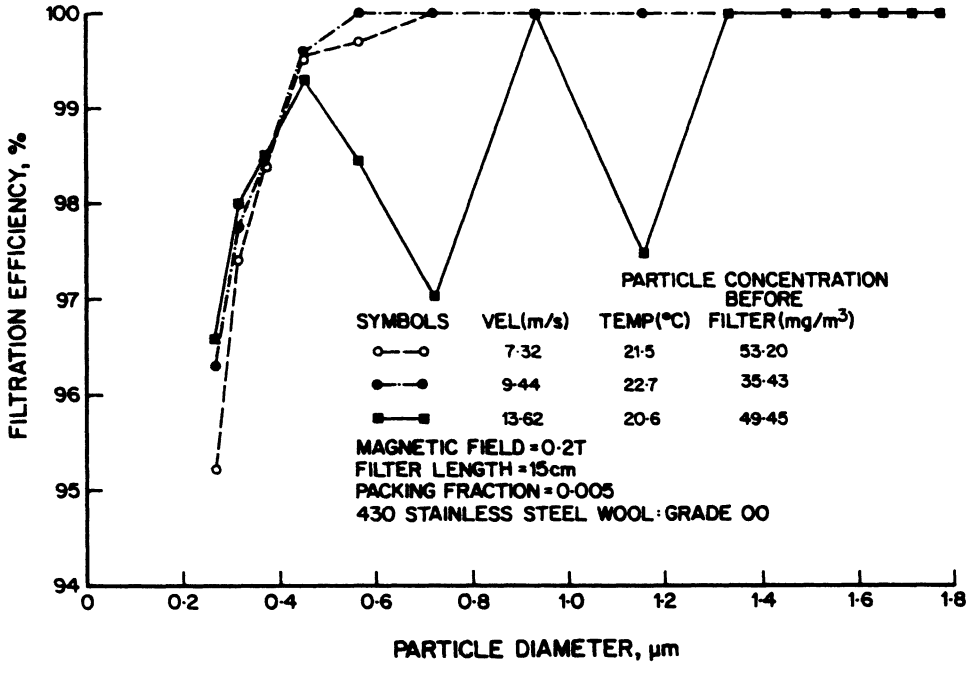

FIGURE 26 Effect of gas velocity on filtration efficiency

increases the filtration efficiency as expected because finer wires offer greater surface for the same packing fraction. But, fine wire (grade 0) aspect ratio 3.55 has lower efficiency than medium wire (grade 2) aspect ratio 2.39. The lower efficiency for the grade 0 wire must probably be due to its higher aspect ratio. This can be explained as follows. Wires of rectangular cross-sections are easily magnetized if the long side lies in the direction of the applied magnetic field but then offers a small target area, and conversely are difficult to magnetize when offering the larger target area. Thus rectangular wires are less effective than square or round wires.

If the front face of the HGMF filter is inspected after loading and with the magnetic field uninterrupted, the dust has

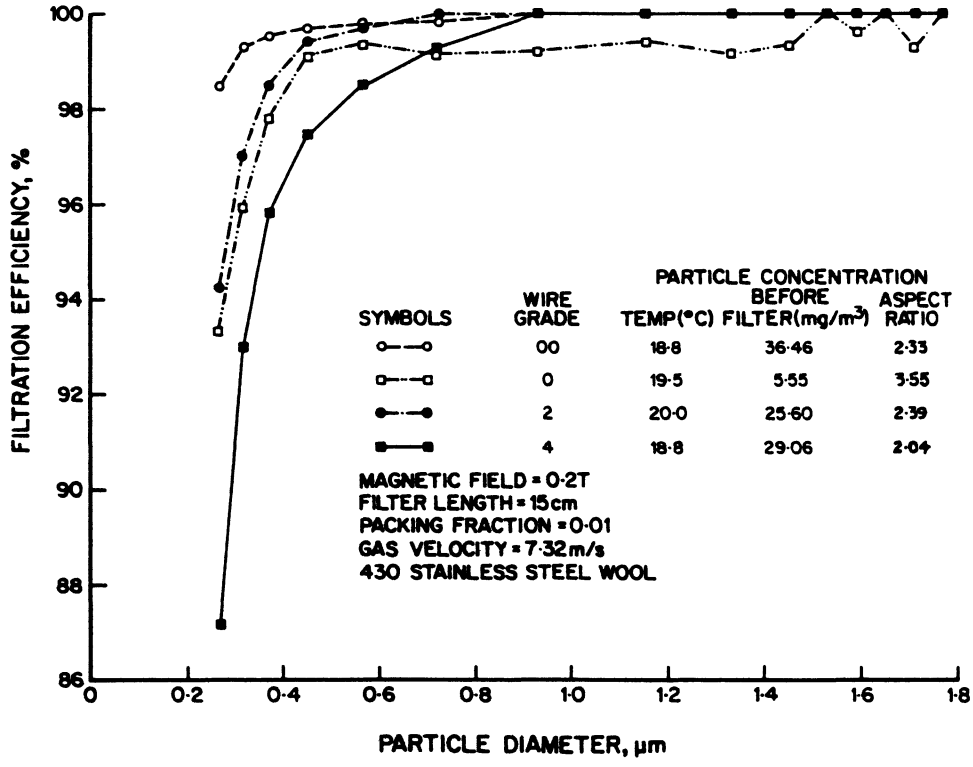

FIGURE 27 Effects of wire size and aspect ratio on filtration efficiency

always collected in the form of spiky structures projecting from the wire. The dust load carried by these spikes on the front wire is, by visual inspection alone, obviously much in excess of that on downstream wires. Although the matrix requires positive cleaning action to remove its dust load, the spikes simply collapse and fall away when the field is removed. By collecting this dust and scraping carefully any remaining material from the front face, the ratio of the mass of dust collected on the front face to that on the rest of the matrix was determined and plotted in Fig. 28 for varying fields at constant velocity and vice-versa. It can be seen that for fields of 0.2T and above, at 7.32 m/s, more dust is collected on the front face than in the body of the matrix. At a constant field of 0.2T, this effect is even more pronounced at low velocity but reduces with increasing velocity.

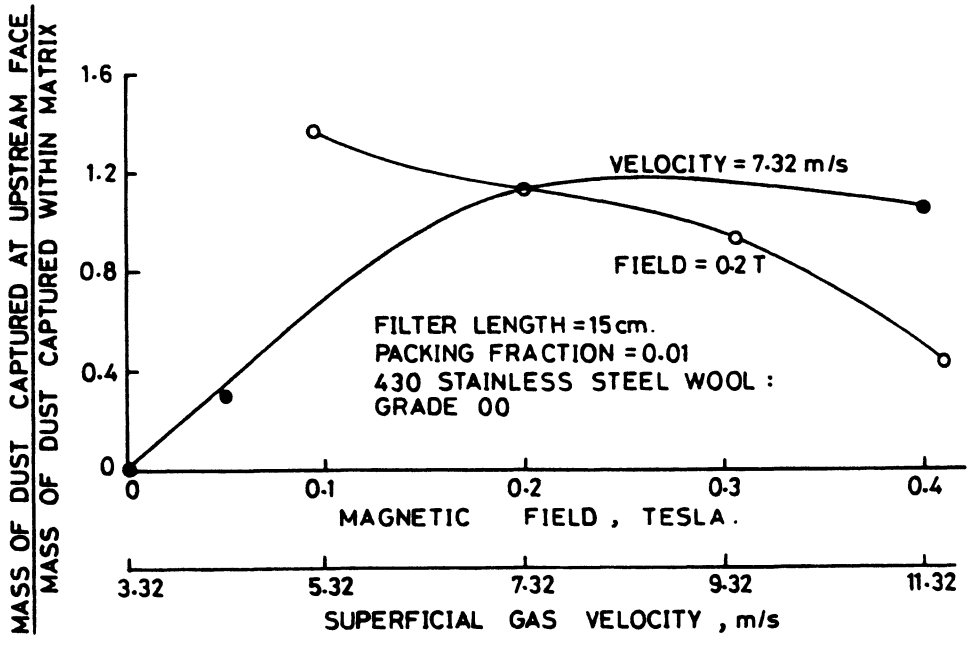

FIGURE 28 Effects of magnetic field and gas velocity on particle capture at upstream matrix face

The mass is concentrated in the smaller numbers of largest particles and the probability of capture of these on the front face is high. The spiky structures suggest that large particles become favourable capture sites for other particles by creating stronger local gradients, thus enhancing the capture radius of the wire and promoting growth at these favourable sites. The front face is additionally favoured by lack of shadowing by or wake effects from upstream wires. The results of Fig. 28 were taken during efficiency tests when the matrix was not heavily loaded. Less complete results taken during the loadability tests (Figs. 17-22) indicate that increasing proportions of dust collect on the front face with increasing matrix loading.

3. ECONOMIC COMPARISON

Preliminary economic estimates by Gooding et al[5] indicate that the capital cost of the HGMF equipment and the power requirements for magnetic field generation and gas movement can be competitive to corresponding air control devices such as electrostatic precipitators and wet scrubbers. The HGMF estimates are based on the filtration of highly magnetic dusts in which high flow velocities are feasible and low magnetic fields (using a conventional solenoid) would be adequate.

REFERENCES

1. R. F. BOUCHER and K. J. BULMER, IEEE Trans. Magn., MAG-18, 6, 1665-1667 (1982)
2. CRC Handbook of Chemistry and Physics, 63rd edition, edited by R. C. Weast (CRC Press, 1982)
3. A. C. LUA and R. F. BOUCHER, IEEE Trans. Magn., MAG-18, 6, 1659-1661 (1982)
4 C. H. GOODING, Pilot-scale Field Tests of High-gradient Magnetic Filtration, U.S. Environmental Protection Agency Report, EPA-600/7-80-037 (March 1980)

5. C. H. GOODING, T. W. SIGMON and L. K. MONTEITH, Application of High-gradient Magnetic Separation to Fine Particle Control, U.S. Environmental Protection Agency Report, EPA-600/2-77-230 (Nov. 1977)
6. FUCHS. N. A.- Aerosol Impactors, Fundamentals of Aerosol Science, edited by D. T. Shaw, (John Wiley & Sons, New York, 1978), Chap.1, pp.1-83
7. A. C. LUA, An Investigation of High Gradient Magnetic Filtration of Fine Particles from Gas Streams, Ph.D. Thesis, Sheffield University (1982)
8. R. F. BOUCHER and A. C. LUA, J. Aerosol Sci., 13, 499-511 (1982)